Research Square

Preprints are preliminary reports that have not undergone peer review.
They should not be considered conclusive, used to inform clinical practice,
or referenced by the media as validated information.

Impact of Shielding Strategies (Wrapping vs. Covering) on Superficial Radiosensitive Organ Doses during Wide- Detector CT Examinations

Dandan Liu
Beijing Tongren Hospital, CMU
Yajian Tong
Beijing Tongren Hospital, CMU
Zixuan Ma
Beijing Tongren Hospital, CMU
Zechen Feng
Beijing Center for Disease Prevention and Control
Jianxing Wu
Beijing Tongren Hospital, CMU
Tongxin Zhang
Beijing Tongren Hospital, CMU
Yuhe Cheng
Beijing Tongren Hospital, CMU
Yuhang Liu
Beijing Tongren Hospital, CMU
Yongxian Zhang
Beijing Tongren Hospital, CMU
Yantao Niu
ytniu163@163.com

Beijing Friendship Hospital

Research Article

Keywords: Wide-detector CT, Shielding protection, Superficial radiosensitive organs, Dose equivalent

Posted Date: July 30th, 2026

DOI: https://doi.org/10.21203/rs.3.rs-9841225/v1

License: This work is licensed under a Creative Commons Attribution 4.0 International License. Read Full License

Additional Declarations: No competing interests reported.

Abstract

Background Protective shielding is a standard practice in CT to reduce radiation exposure to radiosensitive organs. However, its effectiveness on wide-detector CT remains insufficiently evaluated. This study aimed to compare the protective efficacy of two shielding strategies—wrapping and covering—on superficial radiosensitive organs across various scanning protocols using a wide-detector CT scanner.

Methods A total of 402 patients undergoing wide-detector CT examinations (cranial, cervical, lung, abdominopelvic, and coronary CTA) were randomized into wrapping and covering shielding groups. All scans were performed using a 256-row wide-detector CT scanner. Radiation surface doses to the eye lens, thyroid, breast, and gonads were measured using thermoluminescent dosimeters (TLD). The study evaluated internal surface doses beneath shields, external doses, and unshielded organ doses.

Results In cranial axial and helical scans, the wrapping method resulted in significantly higher thyroid surface doses compared to the covering method ($P < 0.001$). In lung and abdominopelvic scans using automatic tube current modulation (ATCM), the unshielded doses to the thyroid and gonads exceeded $CTDI_{vol}$ by approximately 58% and 70%, respectively. A dose inversion phenomenon (internal dose > external dose) was observed in cervical and abdominopelvic scans due to internal scatter accumulation. Compared to helical scans, single-rotation axial scans significantly reduced radiation doses to adjacent organs outside the scan field.

Conclusions The effectiveness of shielding strategies in wide-detector CT is highly site-dependent. The covering method is superior for thyroid protection during cranial scans. Optimization of scanning modes, particularly the use of axial scanning to eliminate z-axis over-scanning, is more critical for organ protection than shielding alone. Due to ATCM and anatomical synergy, $CTDI_{vol}$ alone is insufficient for assessing radiation risks to unshielded organs.

Introduction

Radiation protection in diagnostic imaging is currently undergoing a significant paradigm shift. Numerous professional organizations have recently advocated for the discontinuation of routine patient shielding, citing a lack of robust evidence that it effectively reduces the risk of stochastic effects. Concurrently, rapid advancements in both hardware and software have substantially lowered baseline radiation doses in modern imaging. Furthermore, the improper use of shielding devices can lead to a paradoxical increase in patient dose by interfering with dose modulation systems [1–3]. Furthermore, the risk of disease transmission from pathogens carried by shielding materials has also become a matter of clinical concern.

However, a state of clinical uncertainty remains, as international authorities—including the IAEA, the ICRP, and recent reviews such as that by Schürmann et al. (2026)—note that many national guidelines still recommend shielding for specific superficial radiosensitive organs (e.g., the eye lens, thyroid, breast, and gonads), particularly during high-dose CT examinations [4–6]. Despite the recognized risk of increased dose due to interference with automatic exposure control, the clinical risk-benefit ratio of patient shielding remains poorly defined. This ambiguity highlights an urgent need for individualized, evidence-based shielding guidelines. By critically evaluating existing protocols and addressing the lack of evidence-based risk assessments, clinical radiology can transition toward more tailored practices that enhance overall patient safety.

In this context, the emergence of wide-detector CT (e.g., 256-row scanners) presents new challenges and opportunities, offering broader anatomical coverage and faster acquisition speeds compared with conventional CT [7]. However, its unique radiation distribution—characterized by wide-cone beam geometry and z-axis over-scanning in helical modes—may expose superficial organs to significant radiation doses [8]. Despite these technical distinctions, systematic evaluations of shielding efficacy on wide-detector platforms remain scarce, particularly regarding the comparative performance of "wrapping" versus "covering" techniques. Therefore, this study evaluated the impact of different shielding methods on superficial organ doses across six common examination protocols, aiming to establish an evidence-based foundation for optimized shielding strategies in clinical wide-detector CT practice.

Materials and Methods

Study Design and Population

This prospective study included 404 patients who underwent wide-detector CT examinations at our hospital between May and July 2025. The study protocol was approved by the institutional ethics committee (Ethical Approval Number: TREC2025-KY041), and written informed consent was obtained from all participants. The inclusion criteria were as follows: (1) age ≥18 years; (2) body mass index (BMI) between 15 and 30 kg/m²; and (3) the ability to maintain standard positioning as instructed. Subjects requiring scans beyond the conventional range due to underlying disease or those with metallic implants within the scan field were excluded (n = 2). The final study population consisted of 214 men and 188 women (age range, 18–89 years). The distribution of subjects across examination types was: 50 for cranial axial CT, 81 for cranial helical CT, 66 for cervical CT, 82 for lung CT, 89 for abdominopelvic CT, and 34 for coronary CTA.

CT Scanning Protocols

All examinations were performed using a 256-row wide-detector CT scanner (Revolution CT, GE Healthcare, USA). Automatic Tube Current Modulation (ATCM), especially the Smart mA technique, was applied for neck, lung, abdominopelvic, and coronary CTA protocols to optimize radiation dose based on patient attenuation. The key scanning parameters, including the Noise Index (NI), tube voltage, and tube current modulation ranges (min-max mA), varied by anatomical region and are comprehensively detailed in Table 1. Cranial scans were performed using a fixed tube current protocol. All patients were scanned in the supine position with standardized arm placement as specified in the footnotes of Table 1.

Table 1 Detailed scanning parameters and acquisition protocols for wide-detector CT across different anatomical regions

Scan Protocols	Scout Tube Position	Scout (kV/mA)	kVp	mA range	NI	Focal Spot	Pitch	Collimation (mm)	Direction	Rot. Time (s)	Slice Thickness (mm)	ASiR-V (%)
Cranial Axial Scan	90°	100/10	120	360	-	S	-	160	-	1	5	50
Cranial Helical Scan	90°	100/10	120	300	-	S	0.516:1	40	Foot→Head	0.5	0.625	50
Cervical Scan	90°	120/10	120	Smart 100–450	9	S	0.992:1	80	Head→Foot	0.5	0.625	50
Lung Scan	180°	120/10	120	Smart 150–450	15.7	L	0.984:1	40	Foot→Head	0.5	1.25	30
Abdominopelvic Scan	180°	120/10	120	Smart 250–600	12	L	0.992:1	80	Head→Foot	0.5	1.25	50
Coronary CTA (Calcium Score)	90°+180°	120/10	100	300	-	S	-	160	-	0.28	2.5	50
Coronary CTA (One-beat)	90°+180°	120/10	kV Assist 100	Smart 400–720	14	S	-	160	-	0.28	2.5	50

Abbreviations: ASiR-V, adaptive statistical iterative reconstruction-V; ATCM, automatic tube current modulation; CTA, computed tomography angiography; kVp, kilovolt peak; mA, milliampere; NI, noise index.

Note: Smart mA: Refers to the specific ATCM technique (GE Healthcare) used in this study. mA Range: Values provided (e.g., 100–450) denote the minimum and maximum tube current limits set for the modulation process. Patient Positioning: All subjects were scanned in the supine position. For cranial and cervical scans, the patient's arms were positioned along the sides of the body, with the laser alignment centered at the external auditory canal. For lung, abdominopelvic, and coronary CTA scans, arms were raised above the head to minimize artifacts, with the laser alignment centered at the mid-axillary line. "-" indicates that the parameter was not applicable or not available for the specific protocol.

Randomization and Shielding Protocols

A total of 402 patients were randomly allocated into two shielding groups using a simple randomization sequence generated by SPSS (version 26.0, IBM Corp.). Due to the nature of simple randomization and the sequential enrollment across various examination protocols, the final sample sizes were slightly unequal, with 197 subjects assigned to the Wrapping group and 205 to the Covering group. The shielding devices used in this study consisted of a straight lead thyroid collar (0.59 m × 0.06 m), a large-collar lead thyroid shield (0.59 m × 0.15 m), and four lead aprons (0.5 m × 0.4 m), all maintaining a lead equivalence of 0.5 mm Pb. To minimize inter-operator variability, all shielding devices were positioned by a single senior radiological technologist according to two distinct protocols: in the Wrapping method, the lead collar was tightly wrapped around the neck, and two lead aprons were placed securely on the anterior and posterior surfaces of the subject; whereas in the Covering method, the lead collar and apron were draped over the subject's body, allowing the devices to hang naturally on both sides. Standardization of device placement was based on anatomical landmarks rather than a fixed distance from the scan range to account for variations in patient height and body habitus. For instance, in cervical scans, the upper edge of the lead apron was precisely aligned 2 cm below the sternoclavicular joint. The detailed allocation of subjects across specific examination items (including cranial, cervical, lung, abdominopelvic scans, and coronary CTA), along with the technical specifications and placement criteria for each examination type, are summarized in Table 2.

Table 2 Sample Distribution, Specifications of Shielding Devices, and Anatomical Landmarks for Placement Across Different CT Examination Types

Examination Protocol	Wrapping (*n*)	Covering (*n*)	Target Organs	Shielding Device	Placement Landmark
Cranial Axial Scan/ Helical Scan	28 (Axial) / 42 (Helical)	22 (Axial) / 39 (Helical)	Thyroid	Straight Collar	Centered over thyroid
			Breast	Lead Apron	Upper edge at the sternoclavicular joint
Cervical Scan	33	33	Breast	Lead Apron	Upper edge 2 cm below sternoclavicular joint
			Gonads	Lead Apron	Upper edge at ASIS
Lung Scan	37	45	Gonads	Lead Apron	Upper edge at ASIS
Abdominopelvic Scan	41	48	Thyroid	Large-Collar Lead Collar	Centered over thyroid
Coronary CTA	16	18	Thyroid	Straight Lead Collar	Centered over thyroid
			Gonads	Lead Apron	Upper edge at ASIS

Abbreviations: ASIS, anterior superior iliac spine; CTA, computed tomography angiography; *n*, number of subjects.

Note: Shielding Equivalence: All shielding devices utilized in this study maintained a lead equivalence of 0.5 mm Pb. Placement Landmarks: The anatomical landmarks listed describe the standardized positioning protocol to ensure reproducibility across all participants, accounting for individual variations in patient height and body habitus. Grouping: The sample distribution reflects the number of subjects assigned to each shielding method (Wrapping vs. Covering) within each specific examination protocol.

Dosimetry Measurements

Thermoluminescent Dosimeter Specifications and Processing: Radiation surface doses were assessed using LiF: Mg, Cu, P (GR-200A) thermoluminescent dosimeter (TLD) chips (detection limit: 0.004 mGy). Prior to the experiment, all TLDs underwent a standard annealing process (240°C for 10 min) to standardize sensitivity and eliminate residual signals. Calibration was performed using a X-ray source at beam qualities of 100 kV and 120 kV. TLD readings were obtained using an RE 2000 TLD reader (correction factor 0.91) 24 hours after exposure to minimize potential fading effects. To ensure accuracy, background radiation was monitored and subtracted using 10 control TLDs that were placed outside the scanning room throughout the procedures.

Measurement Sites and Strategy: The selection of measurement sites was tailored to the specific scan range and the proximity of superficial radiosensitive organs. The detailed distribution of measurement sites and the specific quantity of TLDs used for each examination type are summarized in Table 3.

Standardized TLD Placement Procedure: To prevent contamination and ensure measurement stability, all TLD chips were sealed in thin plastic bags prior to placement. The specific placement protocols were as follows: For eye lens: The sealed TLD was affixed to the inner side of the patient's protective eye mask and secured with a disposable tissue to ensure close contact with the eyelid surface. For other organs (thyroid, breast, gonads): The sealed TLDs were attached directly to the skin surface (or the outer surface of the shielding device) at the corresponding anatomical landmarks using medical adhesive tape.

To comprehensively evaluate shielding effectiveness, a dual-measurement strategy was employed for shielded organs (indicated as '4 units' in Table 3):

- Internal (skin) dose: Two TLDs were placed directly on the patient's skin surface (underneath the shielding device) to measure the actual entrance surface dose (ESD).
- External dose: A corresponding pair of TLDs was placed on the outer surface of the lead apron or collar to assess radiation attenuation.

For unshielded organs (indicated as '2 units' in Table 3), a single pair of TLDs was placed on the skin surface. In all cases, TLDs were positioned symmetrically on the left and right sides to account for potential dose asymmetry.

Table 3 Distribution and quantity of TLDs applied to superficial radiosensitive organs across different CT examination protocols

Examination Protocol	Eye Lens	Thyroid	Breast	Gonads
Cranial Axial /Helical Scan	2	4	4	2
Cervical Scan	2	NA	4	4
Lung Scan	2	2	NA	4
Abdominopelvic Scan	2	4	2	2
Coronary CTA	NA	4	NA	4

Abbreviations: CTA, computed tomography angiography; TLD, thermoluminescent dosimeter.

Note: Values represent the total count of TLD chips. 2 (Surface Measurement): One TLD placed on the skin surface on the left and right sides, respectively. 4 (Dual Measurement): Two TLDs on the skin surface (internal, beneath the shielding) plus two TLDs on the shielding device surface (external, for radiation attenuation assessment). **NA**: Not applicable (TLD measurement was not performed for this organ in this protocol).

Statistical Analysis

All statistical analyses were performed using SPSS software (version 26.0; IBM Corp., Armonk, NY, USA). Continuous variables were evaluated for normal distribution using the Shapiro–Wilk test. Normally distributed data were expressed as mean ± standard deviation (SD) and compared between the wrapping and covering groups using the independent-samples t-test. Non-normally distributed data were presented as median (interquartile range, IQR) and compared using the Mann–Whitney U test. Categorical variables were presented as frequencies (n) and compared using the Chi-square test or Fisher's exact test, as appropriate. A two-tailed *P* value < 0.05 was considered statistically significant.

Results

Baseline Characteristics of the Study Population

A total of 402 patients were randomized. As detailed in Table 4, no statistically significant differences were observed between the wrapping and covering groups regarding age, sex, BMI, or radiation dose indices ($CTDI_{vol}$, DLP) across all examination protocols (all $P > 0.05$). For example, in the cranial axial protocol, the mean $CTDI_{vol}$ was 50.58 ± 1.06 mGy for the wrapping group and 51.35 ± 2.98 mGy for the covering group ($P = 0.208$). This baseline comparability ensures that subsequent dose differences are attributable to the shielding methods.

Table 4 Baseline characteristics and radiation dose indices of the study population compared between shielding methods

Examination Site	Shielding Method	Age (years)	Male (*n*)	Female (*n*)	BMI (kg/m²)	$CTDI_{vol}$ (mGy)	DLP (mGy·cm)
Cranial Axial Scan	Wrapping	54.57 ± 17.38	16	12	22.32 ± 2.37	50.58 ± 1.06	809.28 ± 16.95
	Covering	47.77 ± 19.23	14	8	22.29 ± 2.14	51.35 ± 2.98	811.51 ± 17.59
	$t/Z/\chi^2$	1.310	0.216		0.295	-1.275	-1.160
	P Value	0.196	0.642		0.769	0.208	0.257
Cranial Helical Scan	Wrapping	48.45 ± 17.86	25	17	22.54 ± 2.19	44.00 ± 0.18	862.67 ± 48.05
	Covering	49.78 ± 19.71	24	15	22.31 ± 2.27	43.97 ± 0.09	868.10 ± 52.55
	$t/Z/\chi^2$	-0.319	0.003		0.371	0.956	-1.087
	P Value	0.751	0.953		0.711	0.342	0.282
Cervical Scan	Wrapping	51.61 ± 13.94	19	13	22.77 ± 2.85	8.92 ± 0.64	259.58 ± 30.04
	Covering	52.27 ± 12.21	17	16	22.21 ± 2.79	8.89 ± 0.67	258.63 ± 32.03
	$t/Z/\chi^2$	-0.247	0.406		0.474	0.209	0.123
	P Value	0.805	0.524		0.637	0.835	0.902
Lung Scan	Wrapping	52.32 ± 13.44	21	16	23.18 ± 2.39	11.40 ± 2.11	401.88 ± 79.18
	Covering	54.27 ± 12.80	19	26	23.24 ± 1.76	11.25 ± 2.90	390.74 ± 91.93
	$t/Z/\chi^2$	-0.601	1.717		-0.113	0.306	0.552
	P Value	0.550	0.190		0.910	0.760	0.583
Abdominopelvic Scan	Wrapping	58.88 ± 17.11	19	22	24.69 ± 3.83	17.25 ± 3.34	885.32 ± 234.62
	Covering	60.75 ± 15.27	27	21	24.09 ± 3.68	16.19 ± 3.26	833.31 ± 206.48
	$t/Z/\chi^2$	-0.545	0.869		0.751	1.513	1.112
	P Value	0.587	0.351		0.455	0.134	0.269
Coronary CTA	Wrapping	64.00 (57.50, 70.50)	7	9	23.38 (21.71, 24.22)	10.59 (7.52, 17.18)	169.40 (120.17, 274.90)
	Covering	67.00 (59.50, 71.00)	6	12	24.03 (21.66, 25.39)	12.08 (8.86, 18.57)	193.28 (141.74, 297.09)
	$t/Z/\chi^2$	-0.330	0.389		-0.875	-1.353	-1.530
	P Value	0.741	0.533		0.382	0.176	0.164

Abbreviations: BMI, body mass index; $CTDI_{vol}$, volume computed tomography dose index; DLP, dose length product.

Notes: Data Presentation: Data are expressed as mean ± SD for normally distributed variables (age, BMI, $CTDI_{vol}$, and DLP) or median (IQR) for non-normally distributed variables. Statistical Tests: The *t/Z* column presents the statistical value derived from the appropriate test: t denotes the t-statistic from the independent-samples t-test (used for normally distributed data), and *Z* denotes the Z-statistic from the Mann–Whitney U test (used for non-normally distributed data). Significance: *P* values represent the comparison between the wrapping and covering groups using independent-samples t-tests or Mann–Whitney U tests, as appropriate. A two-tailed $P < 0.05$ was considered statistically significant.

Cranial CT: Thyroid and Breast Surface Doses

In both cranial axial and helical scans, the wrapping method resulted in significantly higher thyroid surface doses compared to the covering method (P < 0.001). Axial Scan: The mean thyroid surface dose was 0.98 ± 0.28 mSv in the wrapping group, compared with 0.64 ± 0.14 mSv in the covering group (t = 5.173, P < 0.001). Helical Scan: The median thyroid surface dose was 1.52 mSv (IQR: 1.23–1.93) for the wrapping group, which was significantly higher than the 0.92 mSv (IQR: 0.71–1.23) observed for the covering group (Z = -4.988, P < 0.001).

As shown in Table 5, thyroid surface doses were significantly different from the external doses measured outside the lead collar (P < 0.05), with the wrapping method resulting in higher surface doses compared to the covering method. Regarding breast surface doses, no statistically significant differences were observed between the two shielding methods across both scanning protocols (P > 0.05). Additionally, breast surface doses were significantly lower than the external doses measured outside the lead apron (P < 0.001) (Fig. 1).

Cervical CT: Breast and Gonad Surface Doses

As shown in Table 5, regarding breast surface doses, no statistically significant difference was observed between the wrapping and covering groups (P = 0.069). The median breast surface dose was 0.44 mSv (IQR: 0.35–0.55) for the wrapping group and 0.55 mSv (IQR: 0.42–0.73) for the covering group. Notably, regardless of the shielding method, the surface doses measured underneath the shields were consistently significantly higher than the external doses measured outside the lead aprons (P < 0.05). For gonad surface doses in cervical scans, values for both methods were below the detection limit (LOD) and thus excluded from statistical comparison (Fig. 1).

Lung, Abdominopelvic, and Coronary CTA

Lung CT: No significant difference in gonadal surface dose was observed between the wrapping and covering methods (P > 0.05). Doses in both groups remained at a low level (approximately 0.02 mSv). For both shielding methods, the surface dose measured underneath the shield was consistently lower than the dose measured outside the shield (Table 5).

Abdominopelvic CT: The thyroid surface dose did not differ significantly between the wrapping (0.62 mSv) and covering (0.70 mSv) groups (P = 0.719). However, the dose measured underneath the shield was consistently higher than the dose measured outside the shield (e.g., wrapping group: 0.62 mSv vs. 0.14 mSv) (Fig. 1).

Coronary CTA: Both thyroid and gonadal surface doses were low, with no significant differences found between the different shielding methods (all P > 0.05). Consistent with the findings in Lung CT, the surface doses measured underneath the shield were consistently lower than those measured outside the shield (Table 5).

Table 5 Comparison of surface dose equivalents (mSv) for radiosensitive organs using two shielding methods

Examination Site	Shielding Method (*n*)	Thyroid (Int.)	Thyroid (Ext.)	*P* Value (Thyroid)	Breast (Int.)	Breast (Ext.)	*P* Value (Breast)	Gonads (Int.)	Gonads (Ext.)	*P* Value (Gonads)
Cranial Axial Scan	Wrapping (*n*=28)	0.98±0.28 (*n*=28)	0.79 (0.70, 0.95) (*n*=27)*	<0.001	0.01 (0.01, 0.02) (*n*=23)[5]	0.07±0.01 (*n*=28)	<0.001	/	/	
	Covering (*n*=22)	0.64±0.14 (*n*=22)	0.78 (0.71, 0.88) (*n*=22)	0.001	0.02 (0.01, 0.02) (*n*=19)[3]	0.07±0.01 (*n*=22)	<0.001	/	/	
	P Value	<0.001	0.488		0.662	0.465				
Cranial Helical Scan	Wrapping (*n*=42)	1.52 (1.23, 1.93) (*n*=41)*	0.97 (0.88, 1.14) (*n*=41)*	<0.001	0.02 (0.01, 0.02) (*n*=32)[10]	0.09 (0.07, 0.10) (*n*=41)[1]	<0.001	/	/	
	Covering (*n*=39)	0.92 (0.71, 1.23) (*n*=39)	1.12 (1.00, 1.24) (*n*=39)	0.020	0.02 (0.01, 0.03) (*n*=38)[1]	0.09 (0.08, 0.10) (*n*=39)	<0.001	/	/	
	P Value	<0.001	0.007		0.136	0.577				
Cervical Scan	Wrapping (*n*=33)	NA	NA		0.44 (0.35, 0.55) (*n*=33)	0.36 (0.30, 0.42) (*n*=33)	0.011	<LOD (*n*=0)[33]	0.01 (0.01, 0.02) (*n*=28)[5]	--
	Covering (*n*=33)	NA	NA		0.55 (0.42, 0.73) (*n*=33)	0.49 (0.35, 0.55) (*n*=33)	0.034	<LOD (*n*=0)[33]	0.01 (0.01, 0.02) (*n*=28)[5]	--
	P Value				0.069	0.047		--	0.104	
Lung Scan	Wrapping (*n*=37)	/	/		NA	NA		0.02 (0.01, 0.03) (*n*=36)[1]	0.07 (0.05, 0.09) (*n*=35)*	<0.001
	Covering (*n*=45)	/	/		NA	NA		0.02 (0.01, 0.03) (*n*=45)	0.06 (0.05, 0.07) (*n*=45)	<0.001
	P Value							0.577	0.292	
Abdominopelvic Scan	Wrapping (*n*=41)	0.62 (0.41, 0.95) (*n*=41)	0.14 (0.05, 0.32) (*n*=41)	<0.001	/	/		/	/	
	Covering (*n*=48)	0.70 (0.43, 0.93) (*n*=47)*	0.16 (0.14, 0.24) (*n*=48)	<0.001	/	/		/	/	
	P Value	0.719	0.690							
Coronary CTA	Wrapping (*n*=16)	0.21 (0.15, 0.27) (*n*=16)	0.53 (0.41, 0.83) (*n*=16)	<0.001	NA	NA		0.01 (0.01, 0.02) (*n*=8)[8]	0.05 (0.03, 0.06) (*n*=16)	<0.001
	Covering (*n*=18)	0.25 (0.17, 0.40) (*n*=17)*	0.67 (0.38, 0.94) (*n*=18)	<0.001	NA	NA		0.01 (0.01, 0.02) (*n*=11)[7]	0.05 (0.02, 0.06) (*n*=17)[1]	<0.001
	P Value	0.221	0.597					0.563	0.344	

Abbreviations: Int., internal (measured underneath the shield); Ext., external (measured outside the shield); LOD, limit of detection.

Note: The dose equivalent value is the bilateral average. "/" : Indicates TLD measurement without shielding protection; therefore, these data are not applicable to this table. **NA**: Not applicable (TLD measurement was not performed for this organ in this protocol). "*": Missing TLD measurement data, resulting in a reduced number of cases at this location. Superscript numbers (e.g., [1], [3], [5]): Indicate the number of cases reduced at this location because TLD measurement values fell below the LOD. "--" (in *P* value column): Statistical analysis was not applicable because all recorded values at this site fell below the LOD. All *P* values were calculated using independent-samples *t*-tests or Mann–Whitney U tests; $P < 0.05$ was considered statistically significant.

Unshielded Organs

Regarding the dose levels for unshielded radiosensitive organs (Table 6), statistically significant variations were observed between the shielding groups. In lung CT scans, significant differences in both lens and thyroid doses were noted ($P < 0.05$), with higher values observed in the Covering group. In abdominopelvic CT scans, a statistically significant difference in lens dose was also found ($P = 0.01$), with higher values in the Wrapping group.

Comparison with $CTDI_{vol}$ indicated that in both cranial scan protocols, the median dose equivalent to the unshielded eye lens (40.74 – 47.05 mSv) was comparable to the $CTDI_{vol}$. In lung CT scans, the mean thyroid dose equivalent (17.79 – 21.25 mSv) was approximately 58% higher than the $CTDI_{vol}$ (11.25 – 11.40 mGy). Similarly, in abdominopelvic CT scans, the mean gonadal dose equivalent (27.51 – 29.13 mSv) exceeded the $CTDI_{vol}$ (16.19–17.25 mGy) by approximately 70%.

Table 6 Dose equivalents (mSv) of unshielded radiosensitive organs located within or adjacent to the scan range

Examination Item	Shielding Method	Eye Lens	Thyroid	Breast	Gonads
Cranial Axial Scan	Wrapping (n=28)	42.77 (36.04, 45.93) (n=27)*	†	†	0.02±0.01 (n=25)3
	Covering (n=22)	47.05 (41.15, 50.89) (n=22)	†	†	0.02±0.01 (n=21)*
	P Value	0.165			0.699
Cranial Helical Scan	Wrapping (n=42)	40.74 (38.23, 42.92) (n=42)	†	†	0.02±0.00 (n=37)5
	Covering (n=39)	40.94 (37.79, 44.64) (n=39)	†	†	0.02±0.00 (n=36)3
	P Value	0.571			0.248
Cervical Scan	Wrapping (n=33)	5.70 (4.36, 6.13) (n=33)	NA	†	†
	Covering (n=33)	5.97 (4.84, 6.78) (n=32)*	NA	†	†
	P Value	0.198			
Lung Scan	Wrapping (n=37)	0.63±0.21 (n=37)	17.79±6.16 (n=36)*	NA	†
	Covering (n=45)	0.79±0.21 (n=45)	21.25±6.01 (n=45)	NA	†
	P Value	0.001	0.02		
Abdominopelvic Scan	Wrapping (n=41)	0.20±0.07 (n=41)	†	15.33±7.43 (n=41)	29.13±4.27 (n=41)
	Covering (n=48)	0.16±0.06 (n=47)*	†	12.69±6.84 (n=47)*	27.51±5.15 (n=48)
	P Value	0.01		0.086	0.112

Note: Dose equivalent values represent the bilateral average. "†": Indicates TLD measurement performed with shielding protection; data not applicable to this table. **NA**: Not applicable (TLD measurement was not performed for this organ in this protocol). "*": Indicates missing TLD measurement data, resulting in a reduced number of cases at this location. Superscript numbers (e.g., ³, ⁵): Indicate the number of cases reduced at this location because TLD measurement values fell below the LOD.

Discussion

Principal Findings and General Evaluation

This study utilized a prospective randomized controlled trial to systematically evaluate the protective efficacy of wrapping versus covering shielding strategies for superficial radiosensitive organs during wide-detector CT examinations. Our results demonstrate that shielding effectiveness is characterized by significant anatomical site specificity and technical dependence. Key findings indicate that the covering method provides superior thyroid protection during cranial scans compared to the wrapping method. Furthermore, the single-rotation axial scan mode of wide-detector CT demonstrated a more pronounced advantage in protecting out-of-field radiosensitive organs by eliminating z-overranging, surpassing the efficacy of physical shielding alone. Additionally, in lung and abdominopelvic scans, the synergy between the anatomical site specificity of radiosensitive organs and ATCM technology resulted in radiation risks to unshielded organs that significantly exceeded the console-displayed $CTDI_{vol}$ values.

Mechanistic Analysis of Dose Variations in Superficial Organs

Influence of Shielding Geometry on In-field Organs and Interface Backscatter

In both axial and helical cranial scans, the wrapping method paradoxically led to a significantly higher thyroid dose ($P < 0.001$). This phenomenon is primarily attributed to two deterministic geometric and physical factors. First, the overlapping of the lead collar at the posterior neck in the wrapping method results in a localized doubling of the lead equivalent. Under diagnostic X-ray energy ranges, an increased mass thickness of high-atomic-number materials (lead, Z=82) substantially enhances the photoelectric cross-section, thereby generating a higher level of secondary backscattered radiation at the tissue-lead interface [9, 10]. Second, clinical observations during examinations indicate that the scanning baseline for cranial CT is conventionally set along the orbitomeatal line [11]. Because the gantry of the wide-detector CT is non-tiltable, patients must actively tuck their chins to ensure baseline accuracy. This anatomical positioning inadvertently creates a "geometric gap" between the tightly wrapped lead collar and the skin surface. Under wide-cone beam geometry, these

gaps serve as entrance channels for scattered radiation. In contrast, the conformable covering method closely follows the contour of the patient's anatomy, eliminating both lead overlapping and geometric gaps, thus offering superior thyroid protection.

Impact of Secondary Scatter and Gantry Rotation Dynamics on Distal Organs

In abdominopelvic scans, the lens dose was paradoxically higher with the wrapping method (P = 0.01). Analysis suggests that although the large lead collar used in the wrapping method provides a larger physical protective area, it can simultaneously act as a secondary ionizing radiation source when exposed to the primary high-intensity beam, thereby intensifying scatter propagation toward out-of-field distal organs like the eye lens. This aligns with the findings of Hayre et al., who reported that the use of a 0.35 mmPb lead apron paradoxically increased the radiation dose to adjacent thyroid organs by 20% due to secondary emissions [12]. Furthermore, this variation was compounded by the 360° rotation of the X-ray tube and the inherent randomness of the scanning start and end positions. Due to the irregular geometry of the human cross-section, the attenuation path length of the X-ray beam varies continuously at different rotation angles [13]. This rotation dynamics, superimposed on the secondary scatter contributions from the protective materials, collectively drove the observed statistical differences in lens doses.

ATCM-Driven Dose Compensation in Anatomically Variable Regions

In lung scans, both lens and thyroid doses exhibited higher trends in the covering group; however, this variation was independent of the physical properties of the shielding methods themselves. In this specific protocol, physical shielding was exclusively deployed at the gonadal region—far remote from the head and neck—and no significant difference in $CTDI_{vol}$ was observed between the two shielding groups. The underlying mechanism is driven by the application of ATCM technology in lung scanning. The thyroid is anatomically located at the cervicothoracic junction, a transition zone characterized by dramatic longitudinal and lateral fluctuations in body thickness and tissue density. To maintain the target image quality across these highly heterogeneous sections, the ATCM system automatically and compensatorily ramps up the localized tube current output. This is highly consistent with the simulation study by D'hondt et al., which demonstrated that organ-specific doses to the thyroid in low-dose chest CT are most heavily influenced by patient off-centering and modulation parameter configurations [14]. Consequently, this active tube current compensation generated the observed statistical dose variations in the thyroid and the distal lens. In routine clinical workflows, the inferior pole of the thyroid often borders the margin of the lung imaging field; deploying physical shielding at this boundary would not only introduce severe artifacts and degrade image quality but also directly disrupt the ATCM modulation algorithm, leading to an unintended elevation of the patient's baseline radiation risk.

Impact of Wide-Detector Physical Characteristics on Radiation Dose

The wide-detector CT utilized in this study features a maximum collimation width of 160 mm. When a single-rotation axial scan is employed to cover the target organ, it physically eliminates the z-overranging that is structurally inherent in helical protocols due to continuous table movement. Our results demonstrate that in cranial examinations, although the $CTDI_{vol}$ for axial scans is slightly higher, the radiation dose to adjacent organs outside the scan field (e.g., the thyroid) is significantly lower than that in helical scans due to the elimination of z-overranging . This echoes the pediatric phantom study by Masuda et al., which confirmed that during head CT scans of a 5-year-old phantom, the scattered dose to the thyroid was significantly lower in the axial mode than in the helical mode [15]. Similarly, in the one-beat axial mode of coronary CTA, owing to the complete absence of overranging, both the internal and external scatter doses at the thyroid location remained minimal. Even though the thyroid shield was in close proximity to the imaging field boundary, the internal dose beneath the lead collar remained lower than the external dose, indicating negligible internal scatter and minimal high-Z interface enhancement in this setup. This strongly reinforces the principle that in the modern wide-detector era, optimizing scan modes—specifically prioritizing single-rotation axial volume acquisition—is far more critical for protecting distal radiosensitive organs than relying solely on physical shielding devices [16].

Conversely, a distinct "dose inversion" phenomenon—where the internal dose beneath the shield exceeded the external dose—was observed for the breast in cervical scans and for the thyroid in abdominopelvic scans. Analysis indicates that for both protocols, which utilized an 80 mm collimation width and a pitch near 1.0, the z-overranging induced by helical scanning significantly shortened the physical distance between the primary imaging beam and these superficial organs. Under these conditions, large shielding devices (such as the 15 cm wide lead collar) failed to block the Compton scatter originating internally from the human tissue; instead, they acted as physical barriers that hindered the natural dissipation of internal scatter energy outward, collectively facilitating internal scatter accumulation beneath the shield [17]. Only when organs were structurally remote from the primary imaging volume (e.g., the gonads in lung or coronary scans) did both internal and external scatter doses subside to negligible baseline levels. It is worth noting that the single-piece lead aprons used in this study do not provide 360° wrap-around coverage, which explains the discrepancy between our findings and the paradoxical "higher internal dose" effect reported by Fu et al. regarding full wrap-around protection [17]. Our results align more closely with those of Xin et al., who used Monte Carlo simulations to confirm that for distal organs like the gonads located well outside the scan range, the marginal dose reduction provided by wrap-around lead shielding is essentially negligible [18].

Challenging $CTDI_{vol}$ Conventions: Anatomical Sites and ATCM Compensation

In this study, cranial scans performed without ATCM demonstrated that the median lens dose equivalent was largely comparable to the $CTDI_{vol}$ levels. Within these protocols, the lens dose during helical scans accounted for a higher proportion of the $CTDI_{vol}$ (92% for helical vs. 84%–92% for axial), which is structurally tied to the continuous helical beam trajectory [15]. Conversely, in lung and abdominopelvic scans where ATCM was actively applied, the actual doses delivered to the thyroid and gonads astonishingly exceeded the $CTDI_{vol}$ by approximately 58% and 70%, respectively. This profound dose deviation stems from the synergy between the specific anatomical positioning of these radiosensitive organs and the ATCM modulation logic [1]. The thyroid at the cervicothoracic junction and the gonads in the pelvic region are not merely located at the periphery of intense scatter fields; they represent critical anatomical transition zones with sharp variations in body thickness and tissue cross-sectional density. To maintain the target image quality across these challenging cross-sections, the ATCM system automatically scales up the localized tube current to compensate for tissue attenuation, leading to a

compensatory surge in the dose delivered to these sensitive organs. This finding strongly validates the assertion by the ICRP that $CTDI_{vol}$ primarily reflects the average geometric dose within the direct scan range and is fundamentally incapable of accurately accounting for or representing the true radiation risks to specific organs [5, 19]. Consequently, relying solely on $CTDI_{vol}$ for radiation hazard evaluation and protection strategies in wide-detector CT clinical practice is highly insufficient.

Novelty and Limitations

The novelty of this study lies in its prospective and systematic evaluation of the protective efficacy of wrapping versus covering shielding strategies across various clinical scanning protocols on a wide-detector CT platform. By exploring the complex interactions between shielding modes, variable scanning parameters (axial volume vs. helical, different collimation settings), and sensitive anatomical regions, this research bridges a critical gap in the existing evidence-based literature regarding patient protection in modern imaging environments. Furthermore, the study elucidates the direct intervention mechanisms of ATCM on spatial radiation dose distribution, providing vital support for optimizing radiation protection practices.

Several limitations of this study should be acknowledged. First, the sample size was relatively small and the range of examination protocols was limited, which may partially restrict the universal generalizability of the findings. Second, this study relied primarily on surface dose equivalent measurements to estimate radiation exposure, which possesses physical limitations in fully representing the internal heterogeneous dose distribution within deep organs; thus, future studies utilizing physical anthropomorphic phantoms with internal dosimeter slots are required for further verification. Finally, the research focused on specific hardware configurations and scanning parameters, necessitating additional multi-center investigations into the impact of varying body habitus (BMI) on shielding effectiveness across diverse technical platforms.

Conclusions

In conclusion, this study demonstrates that the impact of shielding strategies on superficial organ doses in a wide-detector CT environment is highly site-dependent. Covering shielding provides superior thyroid protection during cranial scans. Furthermore, the large collimation of wide-detector CT offers a critical advantage for dose optimization: by employing a single-rotation axial scan mode to cover target organs, the system effectively eliminates z-axis over-scanning inherent in helical protocols. This approach significantly reduces the radiation dose to adjacent organs outside the scan field (e.g., the thyroid), demonstrating a protective efficacy that surpasses reliance on shielding devices alone. However, driven by the synergy between anatomical features, 360° tube rotation, and ATCM technology, unshielded organs may still face radiation risks that substantially exceed $CTDI_{vol}$ expectations. Consequently, clinical practice should integrate the optimization of scan modes with a more comprehensive radiation assessment framework, while remaining mindful that shielding organs adjacent to the scan range may induce unintended adverse scatter effects.

Abbreviations

ATCM	Automatic tube current modulation
TLD	Thermoluminescent dosimeter
ASiR-V	Adaptive statistical iterative reconstruction-V
CTA	Computed tomography angiography
kVp	Kilovolt peak
mA	Milliampere
NI	Noise index
ASIS	Anterior superior iliac spine
$CTDI_{vol}$	Volume computed tomography dose index
DLP	Dose length product
Int.	Internal (measured underneath the shield)
Ext.	External (measured outside the shield)
LOD	Limit of detection

Declarations

Acknowledgements

Not applicable.

Author Contributions

DL: Writing – original draft. YT: Data curation, Investigation. JW: Data curation, Investigation. TZ: Data curation, Investigation. ZM: Formal analysis, Data curation. YL: Formal analysis, Data curation. ZF: Investigation, Formal analysis. YC: Investigation, Formal analysis. YZ: Supervision, Writing – review and editing. YN: Supervision, Writing – review and editing. All authors read and approved the final manuscript.

Funding

National Natural Science Foundation of China (82271988)

Data availability

The data that support the findings of this study are available on request from the corresponding author.

Ethics approval and consent to participate

This study was approved by the Ethics committee of the Beijing Tongren Hospital of Capital Medical University(TREC2025-KY041). All methods were carried out in accordance with relevant guidelines and regulations. Informed consent to participate was obtained from all participants prior to their inclusion in the study.

Consent for publication

Not applicable.

Competing interests

The authors declare no competing interests.

References

1. Rautiainen J, Juntunen M, Kotiaho AO. The effect of out-of-plane patient shielding on CT radiation exposure and tube current modulations: a phantom study across three vendors. Radiat Prot Dosimetry. 2022;198(4):229–37.
2. Stearns BK, Seitz K, Folck QM. Exploring Past to Present Shielding Guidelines. Radiol Technol. 2023;95(2):84–93.
3. Begano D, Söderberg M, Bolejko A, TO USE OR NOT, USE PATIENT SHIELDING ON PREGNANT WOMEN UNDERGOING CT PULMONARY ANGIOGRAPHY. : A PHANTOM STUDY. Radiat Prot Dosimetry.2020;189(4):458–465.
4. International Atomic Energy Agency (IAEA). Radiation Protection and Safety of Radiation Sources: International Basic Safety Standards. IAEA Safety Standards Series No. GSR Part 3. Vienna: IAEA; 2014.
5. Commission on Radiological Protection (ICRP). The 2007 Recommendations of the International Commission on Radiological Protection. ICRP Publication 103. Ann ICRP. 2007;37(2–4):1–332.
6. Schürmann T, Lang F, Jakobi A, Rau A, Weiss J, Mueller-Peltzer K, Goller-Bruchmann K, Uller W, Schlett CL, Bamberg F, Fiebich M, Stein T. Paradigm shift in the application of patient contact shielding: a balancing act between tradition and progress. Eur Radiol. 2026;36(3):1709–20.
7. Kang EJ. Clinical Applications of Wide-Detector CT Scanners for Cardiothoracic Imaging: An Update. Korean J Radiol. 2019;20(12):1583–96.
8. Fan Y, Qin T, Sun Q, Wang M, Wang J, Liang B. Measurement of axial dose profile for wide detector CT using radiochromic films. Sci Rep. 2025;15(1):8042. Published 2025 Mar 7.
9. Photon Dose Distributions https://oncologymedicalphysics.com/photon-dose-distributions/
10. Berger T, Vana, Norbert. MEASUREMENTS OF THE DOSE ENHANCEMENT AT THE BORDER BETWEEN METALS AND TISSUE EQUIVALENT MATERIAL. https://www.researchgate.net/publication/242130154
11. National Health Commission of the People's Republic of China. CT examination standard. WS/T 391–2024. Beijing: Standards Press of China; 2024.
12. Hayre CM, Bungay H, Jeffery C. How effective are lead-rubber aprons in protecting radiosensitive organs from secondary ionizing radiation? Radiography (Lond). 2020;26(4):e264–9.
13. Yongxian Z, Yantao N, Senlin G et al. Influence of CT scanning mode on the variability of radiation dose measurements of superficial organs[J]. Chin J Radiological Med Prot 2021,41(12):956–60.
14. D'hondt L, Haentjens C, Kellens PJ, Snoeckx A, Bacher K. Influence of Off-Centre Positioning, Scan Direction, and Localiser Projection Angle on Organ-Specific Radiation Doses in Low-Dose Chest CT: A Simulation Study Across Four Scanner Models. J Imaging. 2026;12(3):123.
15. Masuda T, Kiguchi M, Fujioka C, Oku T, Ishibashi T, Katsunuma Y, Yoshitake T, Abe S, Awai K. Comparison of pediatric lens scattered dose measurements between axial 40-mm and helical 160-mm detector width computed tomography scan modes. Pediatr Radiol. 2024;54(7):1197–204.
16. Schilham A, van der Molen AJ, Prokop M, de Jong HW. Overranging at multisection CT: an underestimated source of excess radiation exposure. Radiographics 2010 Jul-Aug;30(4):1057–67.
17. Qiang F, Lu W, Yue X et al. Study on the effect of personal radiological protective equipment used in diagnostic radiology. Chin J Radiol Med Prot 2023,43(6):462–8.
18. Xin L, Zhuo W. Simulation of the shielding effect of lead apron undergoing chest CT scan. Radiat Prot Dosimetry. 2024;200(16–18):1554–60.

19. Sources, Effects and Risks of Ionizing Radiation. UNSCEAR Report No. 2019. Report to the General Assembly Scientific Annexes A and B. United Nations: United Nations Scientific Committee on the Effects of Atomic Radiation (UNSCEAR); 2020.

Figures

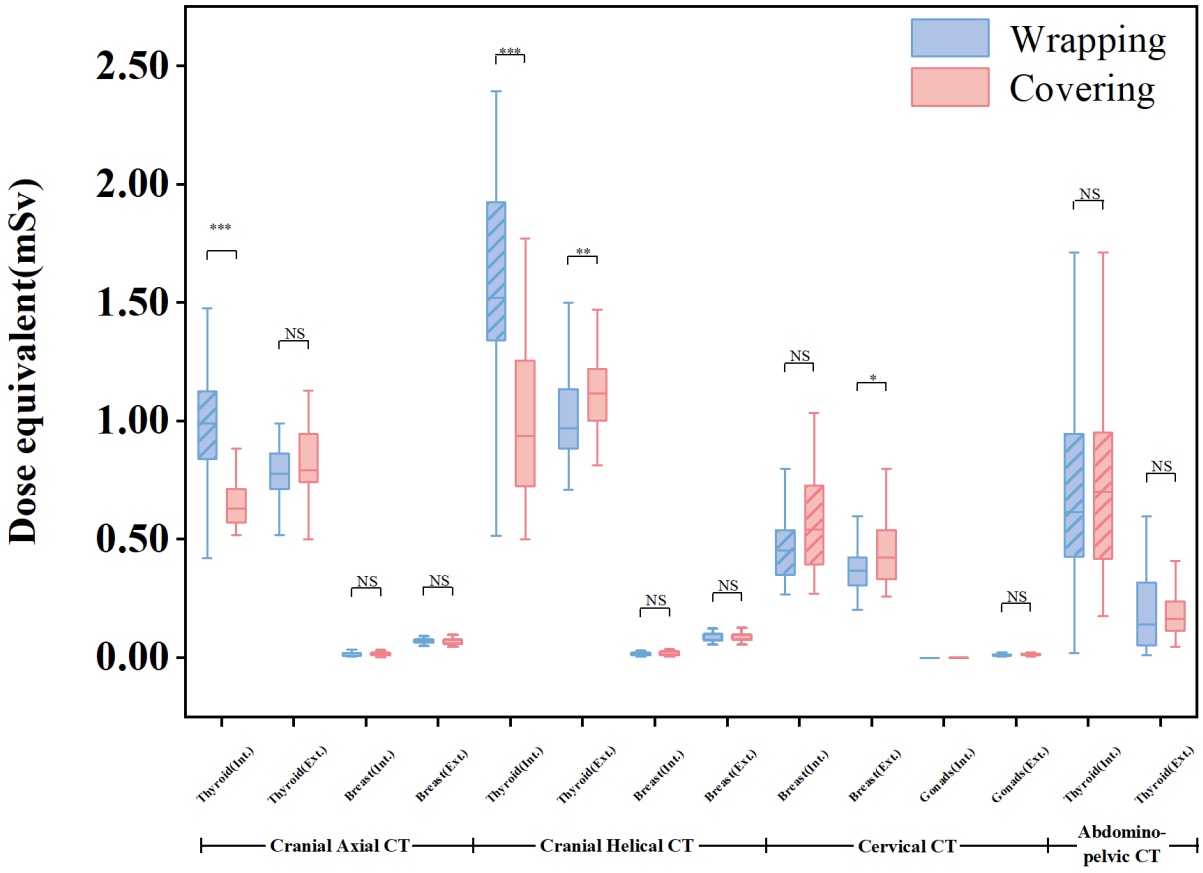


Figure 1

Internal and external dose equivalents of shielded radiosensitive organs in cranial, cervical, and abdominopelvic CT scans. *P < 0.05, **P < 0.01, ***P < 0.001, NS, no statistical significance. Diagonal slashes indicate that the surface dose measured underneath the shield was higher than the dose measured outside the shield.